Materials Science-Poland, 40(3), 2022, pp. 135-151
http://www.materialsscience.pwr.wroc.pl/
DOI: 10.2478/msp-2022-0038

Effect of shot peening on corrosion resistance of additive manufactured 17-4PH steel

Aleksander Świetlicki[1,*], Mariusz Walczak[1], Mirosław Szala[1]

[1]Department of Materials Engineering, Faculty of Mechanical Engineering, Lublin University of Technology, Nadbystrzycka 36, 20-618 Lublin, Poland

Components produced by additive manufacturing (AM) via direct metal laser sintering (DMLS) have typical as-fabricated surface defects. As a result, surface properties of AM products should be modified to increase their strength, anti-wear behavior, and at the same time ensure their high corrosion resistance. Surface modification via shot peening (SP) is considered suitable for AM of engineering devices made of 17-4PH (X5CrNiCuNb16-4) stainless steel. The objective of this study was to determine the effect of three types of peening media (CrNi steel shot, glass, and ceramic beads) on the corrosion resistance of specimens of DMLS 17-4PH stainless steel. Results demonstrated that SP caused steel microstructure refinement and induced both martensite (α) formation and retained austenite (γ) reduction. 17-4PH specimens peened showed the increase in surface hardness of 255, 281, and 260 $HV_{0.2}$ for ceramic, glass, and steel, respectively. DMLS 17-4PH specimens modified by SP exhibited different surface morphology, hardness, and microstructure and thus, these properties affect corrosion performance. The results implied that steel shot peened with steel shot showed the highest resistance to corrosion processes (I_{corr} = 0.019 μA/cm^2), slightly worse with glass (I_{corr} = 0.227 μA/cm^2) and ceramics (I_{corr} = 0.660 μA/cm^2) peened. In the case of ceramic and glass beads, it was possible to confirm the presence of the above-mentioned particles in the surface layer after SP.

Keywords: *additive manufacturing, microstructure, shot peening, stainless steel, corrosion*

1. Introduction

Steel 17-4PH (UNS S17400, AISI 630, 1.4542) has found applications in the chemical, aerospace, energy, marine, and biomedical sectors [1]. It is one of the frequently used steels for precipitation hardening and fabrication of injection molds [2]. The group of precipitation hardening steels was created as a result of the demand associated with World War II for inexpensive materials with high strength at elevated temperatures [3]. The strengthening mechanism is based on precipitation of highly dispersed copper particles in the martensitic phase [4]. Martensitic steel has a predominantly austenitic matrix at solutionizing temperatures of approximately 1,040–1,065°C, while the process of cooling to room temperature triggers a transformation that turns it into a martensitic phase [5].

Shot peening (SP) is a common treatment used to increase the strength and fatigue life of metal components [6]. The strengthening occurs by introducing compressive residual stresses in the near-surface layer and increasing the dislocation density [7]. With SP, hardness, roughness, and corrosion resistance can be modified [8]. SP can increase fatigue resistance, resistance to fretting, rolling contact fatigue, or resistance to stress corrosion cracking [9].

SP is based on imparting particles with a spherical or near-spherical shape with sufficient velocity so that they are able to plastically deform the surfaces of the component being modified. By deforming the material, residual compressive stresses are generated in the material, and strengthening by crushing and fragmentation of grains within the surface layer takes place. A schematic representation of the changes within the surface layer is shown in Figure 1. As can be seen in Figure 1, SP can close cracks formed in the manufacturing process [10]. Shots can be made, for example, from steel, glass, ceramics, or nutshells [11]. Particle acceleration is accomplished typically using compressed clean air. During the flight, the particles

* E-mail: aleksander.swietlicki@pollub.edu.pl

© Świetlicki et al. 2022. This is an open access article distributed under the Creative Commons Attribution-NonCommercial-NoDerivatives 4.0 License. (http://creativecommons.org/licenses/by-nc-nd/4.0/)

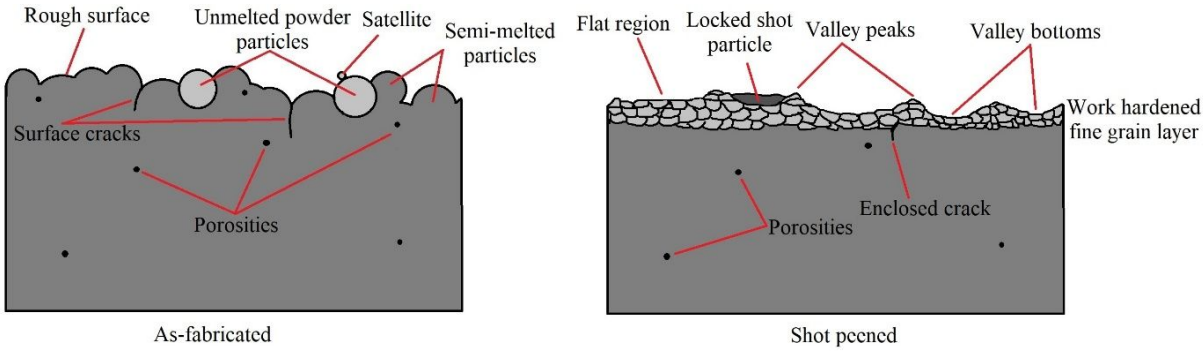

Fig. 1. Schematic of changes within the surface layer of the material following fabrication and after peening, compiled on the basis of [13]

collide with each other as well as with the surface of the component being processed [12].

Additive manufacturing (AM) is an innovative manufacturing method that converts a three-dimensional (3D) CAD digital model into a physical model [14]. Manufacturing involves dividing the model into slices and subsequently fabricating layer by layer [15]. However, additively manufactured steel is not free of discontinuities, pores, sometimes unmelted particles, and so on, which can directly affect corrosion resistance. In addition, the direction of fabrication can affect porosity [16]. Therefore, other treatments are often used to improve these properties [17]. Another characteristic is the lower density of the material, as studies have confirmed that SP is an effective treatment for increasing the hardness of the material, particularly when combined with precipitation hardening [18].

For 17-4PH steels, precipitation hardening, that is, solution treatment combined with aging, is often used. These treatments are aimed at dissolving the intermetallic phase and increasing hardness. In 17-4PH steel, there are usually two phases, martensite and austenite, and the austenite can be either primary or reversed [19]. In some studies, ferrite was also detected after AM.

The structure of 17-4 PH steel may contain both austenite and martensite. It is worth noting here that SP can lead to strain-induced transformation of austenite to martensite [20]. Both indirect and direct transformations have been observed. However, the most common transformation is the γ-ε-α' transformation. Above that, SP around improves stress-corrosion, corrosion, and fatigue properties. However, it can be a detrimental process when high cyclic stresses are present [21]. The biggest impact on the phase composition is due to the manufacturing technology, as well as the material or gases used (for atomization and as a shielding gas) [22]. According to Starr et al. [23], the use of nitrogen atomized powder in an argon atmosphere had little effect, as the material was more than 96% austenitic. However, the same (nitrogen atomized) powder when produced in a nitrogen atmosphere resulted in an austenite content of 99.3%. Using powder atomized in argon and fabricating in nitrogen resulted in 76% martensite content. Using both atomization and fabrication in an argon atmosphere, 87% martensite was obtained. Rafi et al. [24] also confirmed this relationship regarding phase composition. In addition, the hardness was examined, in the as-fabricated state; the highest hardness was found in steel from powder atomized in nitrogen and produced with an argon atmosphere around 280 HV. The lowest hardness of around 230 HV was obtained in the nitrogen–nitrogen regime.

17-4PH steel has relatively good corrosion resistance comparable to duplex (austenitic–ferritic) steels. Guo et al. [25] compared the resistance of AISI 304 steel with 17-4PH; however its mechanical properties and hardness were found to be higher. Most of the information that can be found on 17-4PH steel is similar and describes the resistance as similar to 304 in most environments; in some, however, it shows slightly better properties. However, the resistance of the steel after AM may

differ from materials produced by classical manufacturing methods. Thus, the corrosion properties of steel can be affected by the conditions of manufacturing and processing. Stoudt et al. [26] noted the hazards that can occur in environments in which chloride and halide ions are present. Despite the good resistance of this group of steels in aerated aqueous environments, localized attacks can occur. The corrosion resistance of stainless steels comes from a thermodynamically stable Cr-rich passivating oxide layer. Steel 17-4PH has the best corrosion resistance in dilute aqueous solutions in the group of hardened stainless steel alloys [27].

Lara Banda et al. [28] studied the passivation of 17-4PH steel in citric acid. They found that by passivating in citric acid, it was possible to produce a passivation-resistant layer in the presence of sodium chloride (NaCl) and sulfuric acid H_2SO_4. Karaminezhaad et al. [29] conducted a study on the effect of molybdenum on stress corrosion cracking for 17-4PH steel. They found that I_c and I_{pass} decrease with increasing Mo content. Moreover, it was found that the extent of passivation increases with an increase in molybdenum content. Moreover, its addition does not facilitate the formation of an oxide layer and increases resistance to pitting corrosion. Tavares et al. [19] conducted a research on the effect of sulfur on the corrosion resistance of 17-4PH steel. Two samples with very low and acceptable sulfur content after different heat treatments were investigated. The degree of sensitization (DOS) was higher for samples in the high-sulfur H900 condition due to preferential attack on MnS inclusions. Intergranular corrosion was also detected in the H1150 state due to the precipitation of chromium carbides and the formation of reverse austenite. H900 condition indicates aging at 900°F for 1 hr and in H1150 it indicates aging in 1,150°F for about 4 hr. In addition, all high-sulfur samples had lower pitting potentials (E_{pit}) than low-sulfur samples. 17-4PH steel is often used in gas and oil production systems, and acidic environments such as H_2S, CO_2, and/or water are present [30]. 17-4PH steel is subject to sulfide stress cracking. In this type of cracking, environmental factors such as temperature, molecular pressure of H_2S, pH of the environment, or the presence of chlorides have the greatest influence.

Nakhaie and Moayed [31] studied the resistance of 17-4PH steel to pitting corrosion after cold rolling. They found no significant effect on the potential for pitting. However, cold rolling was found to increase the dissolution rate of metastable pitting in a way that facilitated the transition from metastable to stable pitting. Raja and Rao [32] studied the behavior of welded joints, and found that better corrosion resistance was exhibited by steel after solution treatment and aging at the highest temperature than by solutionized steel. In the case of steel after the welding process, pitting was found at the boundary of d-ferrite and martensite and in the heat affected zone at the grain boundary. Kosasang et al. [33] investigated the effect of aging on the corrosion resistance of 17-4PH steel in artificial salvia. Pitting corrosion occurred where pores were already present. The mechanism was determined to be a two-stage process; in the first stage, dense corrosion products are formed followed by accelerated dissolution by peeling. The highest resistance was obtained with aging at 480°C in both electrochemical measurements and the immersion test. Barroux et al. [34] studied the pitting corrosion resistance of 17-4PH steel fabricated by laser beam melting (LBM) technique and found that the pitting initiation points were lack-of-fusion pores. However, they did not affect the overall corrosion resistance due to their small number and when considering i_{pass} and E_{pit}, the LBM-manufactured steel exhibited better properties than the wrought material. Differences in the behavior of individual pits in additively manufactured versus wrought material were also indicated. Metastable pits formed on LBM were very few, characterized by long lifetimes and large amounts of charge, while wrought presented more metastable pits with short lifetimes and small amounts of charge.

Corrosion resistance can be affected by the scanning strategy in AM in powder bed fusion processes [35]. The use of concentric scanning can improve corrosion resistance by up to about 30%. The use of double scanning or hexagonal strategy did not result in changes in corrosion resistance. However, the impact is not fully investigated and further research should be conducted in this field.

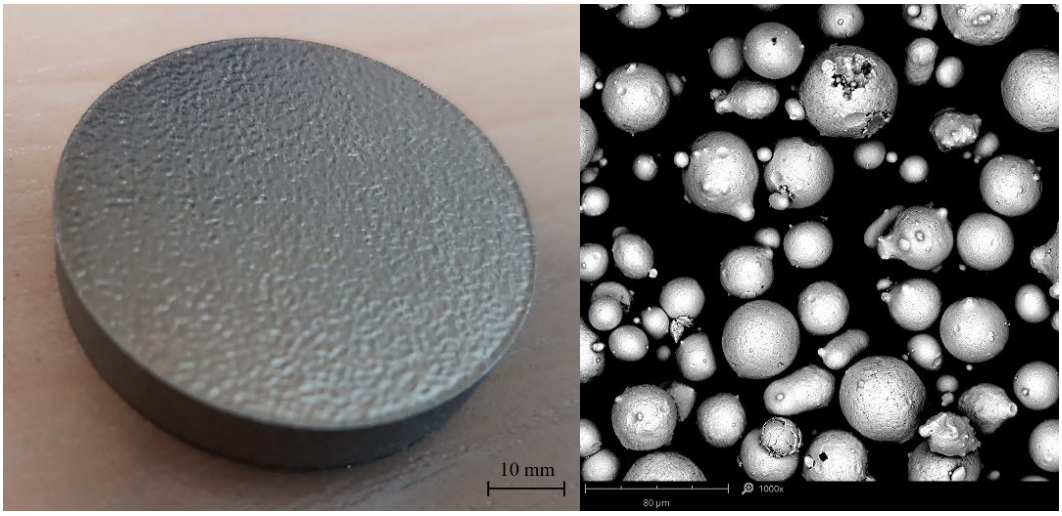

(A) (B)

Fig. 2. 17-PH: (A) DMLS printed specimen's texture after SP; (B) EOS GP1. DMLS, direct metal laser sintering; SP, shot peening

SP-induced changes in the surface layer, as well as changes in the microstructure, can potentially affect the corrosion resistance of steel. During cold processing, a transformation of metastable austenite into martensite and intermediate carbides like Fe_3C called "Martensitic stress-induced transformation" (MIST) can occur [36], which can affect corrosion resistance. One of the dangers during SP is the potential penetration of burnishing medium particles into surfaces, thus reducing or increasing corrosion resistance. It was also found that treatment in solution followed by peak aging increased the resistance of the weld and the material within the heat affected zone [32].

Since AM is a completely different method from conventional ones, the 17-4PH grade is characterized by a complexity of structures depending on the implemented process. As far as the authors' knowledge goes, there are no studies depicting the SP of 17-4PH steel with glass beads often used in the manufacture of injection molds as well as describing the corrosion behavior of 17-4PH steel after the SP process. This paper attempts to answer the question of how the corrosion resistance of 17-4PH steel changes after SP, as well as how its operating properties such as hardness and roughness change. This work aims to assess how corrosion resistance may be affected by particles locked in surface, and which penning parameters are most appropriate, that is, particle size and pressure.

2. Methods

The test object was X5CrNiCuNb16-4 (17-4PH) steel samples printed from GP1 metal powder manufactured by EOS (see Figure 2B). The chemical composition of the test specimens is shown in Table 2. The 3D printing process was carried out in direct metal laser sintering (DMLS) technology. EOSINT M280 device was used (from EOS GmbH) using optimal printing parameters from EOS′ closed software license, among others: laser power was 200 W, sintering thickness was 0.02 mm, and laser spot size was 0.1 mm. The particle of GP1 powder that was used was of the order of 10–50 µm on average. Powder particles were characterized by mostly spherical shape with some satellites. Nitrogen was used as a shielding gas for fabrication.

Four cylindrical test specimens were made and cleaned with compressed air and by ultrasonic cleaning. The specimens of 17-4PH steel were in the shape of disks with dimensions of ⌀30 mm and H = 6 mm. The appearance of the samples and GP1

Table 1. Specimen's designations and peening characteristics

Peening medium	Size of particles [μm]	Time [min]	Peening pressure [MPa]	Chemical composition
Reference	–	–	–	–
Ceramic	⌀125–250	1	0.3	ZrO_2 60%–70%, SiO_2 28%–33% $Al_2O_3 < 10\%$
Glass beads	⌀100–200	1	0.3	70% SiO_2, 10% CaO, 15% $Na_2O + K_2O$, 5% MgO
Steel shots	⌀400–900	1	0.3	Cr 16%–20%, Ni 7%–9%, Si 1.8%–2.2%, Mn 0.7%–1.2%, C 0.05%–0.02%, Fe-Bal.

powder is shown in Figure 2. The chemical composition of the tested steel is given in Table 1.

The external surfaces of the specimens in the *X*–*Y* horizontal plane were subjected to SP (perpendicular to the surface) using Lepco's Peenmatic micro 750S. Three different sphere-like media were used for SP: ceramic beads, glass balls, and CrNi steel shot. A peening pressure of 0.3 MPa was applied and the surface treatment time was 60 s. The distance from the nozzle to the face of the specimen's surface was constant at 20 mm. The characteristics of the modified specimens and the designations adopted in the work are given in Table 1.

2.1. Chemical composition analysis

A Magellan Q8 spark emission spectrometer (Bruker, Germany) using the Fe130 software was used to determine the chemical composition. Five tests (sparks) were performed for each sample to confirm that the composition complies with the manufacturer's declarations and the requirements outlined in ASTM A564 and EN10088-1.

2.2. Hardness

Hardness tests were carried out on a Future-Tech FM-800 microhardness tester at a load of 1,961 N and dwell time of 15 s. Sixteen indentations were made for each sample starting from the surface down to a depth of about 300 μm. The indentations were made at an interval of about 20 μm. Surface hardness was also measured using Future-Tech FM-800 microhardness tester under load condition.

2.3. Roughness

To determine the effect of peening on roughness, roughness tests were conducted using a Dektak 150 contact profilometer (Veeco Instruments, USA). Measurements were made using a stylus with a rounding radius of 2 μm at a measuring length of 5 mm and under a load of 3 mg. Twelve measurements were made for each sample at randomly selected locations. To account for the effect of texture, 12 measurements were taken: 6 along and 6 perpendicular to the scanning direction of the laser beam. The average value was then calculated. To compare different DMLS samples, the average surface roughness was determined based on the arithmetic mean of R_a, R_q, and R_t roughness according to ISO 4287.

2.4. Microstructural characterization

Preparation for testing was done by cutting the disks after peening and preparing the metallographic specimens. The specimens were ground on papers ranging from #600, #800, and #1,200 grit and polished with a 3-μm diamond suspension. Etching was carried out in Kalling's 1 reagent, after which the samples were polished again. Reagent selection was based on ASTM E407-07(2015).

The phase composition of both unpeened and shot-peened specimens, as well as their grain size development caused by different peening parameters were investigated using a high-resolution X-ray diffractometer (XRD, Empyrean, Panalytical) with Cu K-α radiation and Ni-filter with a generator voltage of 40 kV and a current of 30 mA. A proportional detector was used for detecting radiation. The specimens were measured in the Bragg–Brentano geometry over a range from 30° to 100°.

Table 2. Chemical composition in accordance with manufacturer data and ASTM A564

		C	Cr	Ni	Cu	Mn	Si	Mo	Nb	Fe
17-4PH as-fabricated	Wt. [%]	0.04	15.85	4.92	4.79	0.67	0.71	0.12	0.27	Bal.
GP1		0.01	15.8	4.02	3.9	0.7	0.7	0.4	0.29	Bal.
GP1 powder (EOS declaration)		<0.07	15–17.5	3–5	3-5	<1	<1	<0.5	0.15–0.45	Bal.
EN10088-1		<0.07	15–17	3–5	3-5	<1.5	<0.7	<0.6	5*C–0.45	Bal.
ASTM A564		<0.07	15–17.5	3–5	3–5	<1	1	<0.5	0.15–0.45	Bal.

All measurements were carried out at room temperature with a step size of 0.01° and a counting time of 6 s per data point. Specimen phase and lattice parameters from d-spacing were determined with the use of the High Score Plus software package (Panalytical). Crystallite size was calculated according to Scherer equation.

2.5. Scanning electron microscopy-EDS analyses

Scanning electron microscopy (SEM) was used to observe changes in the surface layer. A Phenom world ProX scanning microscope was used. The energy dispersive X-ray spectroscopy (EDS) detector on a Phenom ProX microscope was used to determine the phase composition on the surface after SP. Tests were conducted in areas where pitted shot residues may have been present. Peened surfaces were examined with the SEM-EDS using backscattered electrons (BSD) in SEM imaging and topographic modes.

2.6. Corrosion testing

Evaluation of the corrosion resistance of the test specimens was determined through accelerated electrochemical tests in a 3.5% NaCl solution using the Atlas 0531 corrosion test kit. The tests were conducted at room temperature of 22°C in a three-electrode electrochemical tank, where the control electrode was a platinum electrode, and the reference electrode was a saturated calomel electrode (SCE). The surface area of the electrode under test was 0.5 cm^2. The polarization curves were recorded with an automatic potential shift of 1 mV/s in the range from -500 mV to +600 mV. The corrosion current density I_{corr}, corrosion potential E_{corr}, and pitting potential E_p were determined from the Tafel curves through the analysis of potentiodynamic curves in the AtlasLab software.

3. Results and discussion

3.1. Analysis of the chemical composition

Chemical composition tests showed that the chemical composition is in accordance with the manufacturer's declarations of the requirements given in ASTM A564 and EN10088-1. The results of the chemical composition tests in weight percent are shown in Table 2.

3.2. Hardness

Figure 3 shows the hardness profiles reaching a depth of about 300 μm.

The glass beads peened sample had the highest average surface hardness. The smallest surface hardness was exhibited by the non-peened sample, as seen in Figure 4.

Hardness tests, along with metallographic studies, made it possible to determine the thickness of the reinforced layer. For the Reference sample, the hardness was similar for the entire cross section. After SP with ceramic particles, strengthening was achieved in the material to a depth of 40 μm. After SP with glass beads, the level of strengthening was found to be 60 μm. On the other hand, SP with steel shot produced the best result in the form of a layer strengthened to about 80 μm. It should be noted at this point that these are approximate average values.

Qin et al. [9] conducted a study on SP and thermal stress relaxation. SP was carried out at different pressures of compressed air, steel cut wire shot

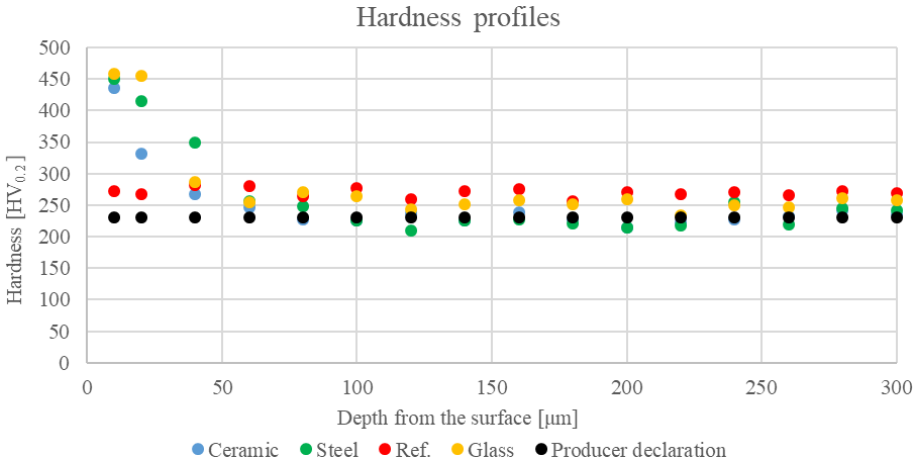

Fig. 3. Hardness profiles of SP specimens. SP, shot peening

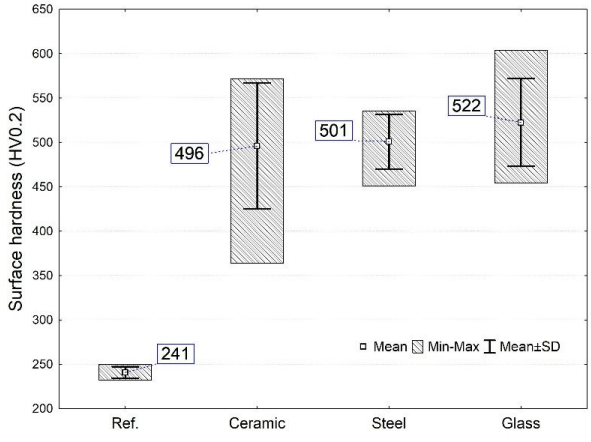

Fig. 4. Surface hardness of un-peened and shot peened 17-4PH

was used in the process, and the coverage area was 200%. Hardness was determined by microindentation and was found to increase from about 3 GPa for the native material to about 4 GPa after SP. Eskandari et al. [37] obtained a hardness after fabrication of 269 ± 34 HV compared with 339 ± 79 HV for the forged material. The variations within the hardness are related to the presence of pores, voids, phase composition, and microstructure. Research by Wang [38] demonstrated that SP has made in 17-4PH steel changes within the size of domains, dislocation density, and microcracks. Changes in the surface region after the SP process are mainly related to the high density of dislocations in the surface layer and the fine size of the domains. In the microstructure, the sliding movements of dislocations at the microstructure boundary are blocked and in the altered layer these movements are hindered, resulting in an increase in fatigue life.

3.3. Roughness

Mathoho et al. [39] conducted roughness analysis for 17-4PH steel produced by laser engineered net shaping (LENS) technique. After laser peening, the roughness decreased after 3 and 6 passes by 28% and 42%, respectively. Hardness at a depth of about 25 µm after 6 passes of laser peening was also examined, and an increase in roughness was found from 374 to 397.67 HV.

Qin et al. [9] determined R_a after peening to be 2.47 ± 0.23, 3.38 ± 0.47, and 3.91 ± 0.36 µm for pressures of 0.24, 0.40, and 0.52 MPa, respectively, and a coverage area of 200%. Roughness parameters after SP depend on parameters such as peening pressure, material hardness, applied medium, or nozzle distance, but also coverage area [40]. By using SP, it is possible to remove tool marks as well as reduce roughness parameters such as R_a and thus increase fatigue strength and remove crack initiation points [41]. The results of the roughness tests are presented in Figure 5, where SD is the standard deviation. Figure 5 shows the values of the parameters R_a, R_q, R_t, R_v, and R_p, respectively, the arithmetic mean roughness, root-mean-square roughness, total height of profile, depth of valleys, and the heights of peaks.

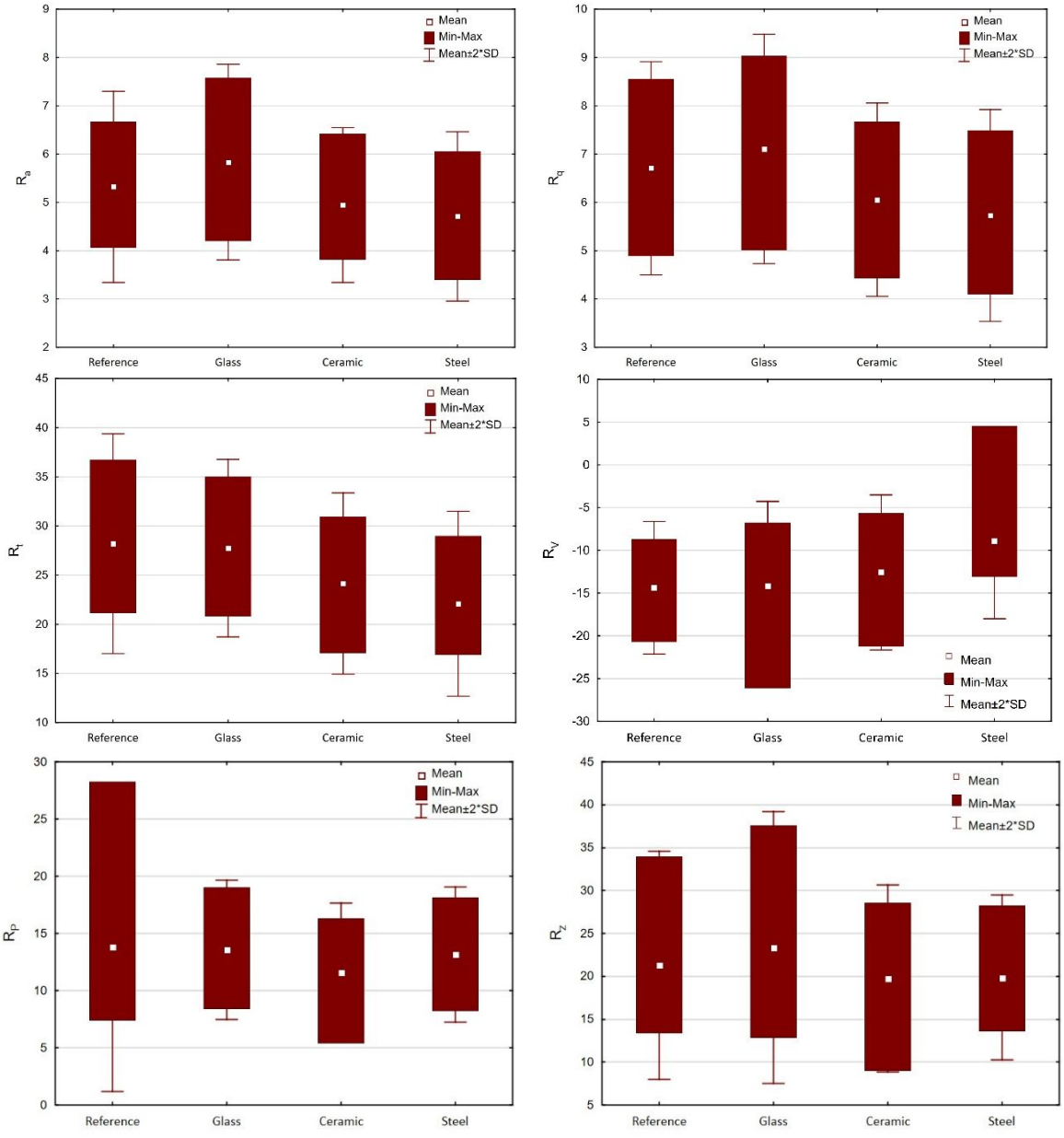

Fig. 5. Roughness parameters (A) R_a, (B) R_q, (C) R_t, (D) R_v, (E) R_p, and (F) R_z

In a previous publication [42], two different SP pressures of 0.3 and 0.6 MPa and three SP media of steel balls, ceramic bead, and nutshells were used. In the previous work, different peening pressures and different peening media were used. That work was aimed more to access wear resistance. In this manuscript, hardness profile measurements and metallographic cross-section imaging are shown; constant peening pressures were used and glass bead instead of nutshells. Comparing the results of the roughness test after SP, it can be concluded that the roughness obtained after fabrication was similar to previously obtained R_a 5.05 $\pm$ 1.02. In contrast, roughness decreased after SP with ceramics and steel. R_a dropped to a value of 7% and 12%, respectively, compared with the reference sample. Applying glass beads for SP resulted in a 10% increase in R_a compared with the refer-

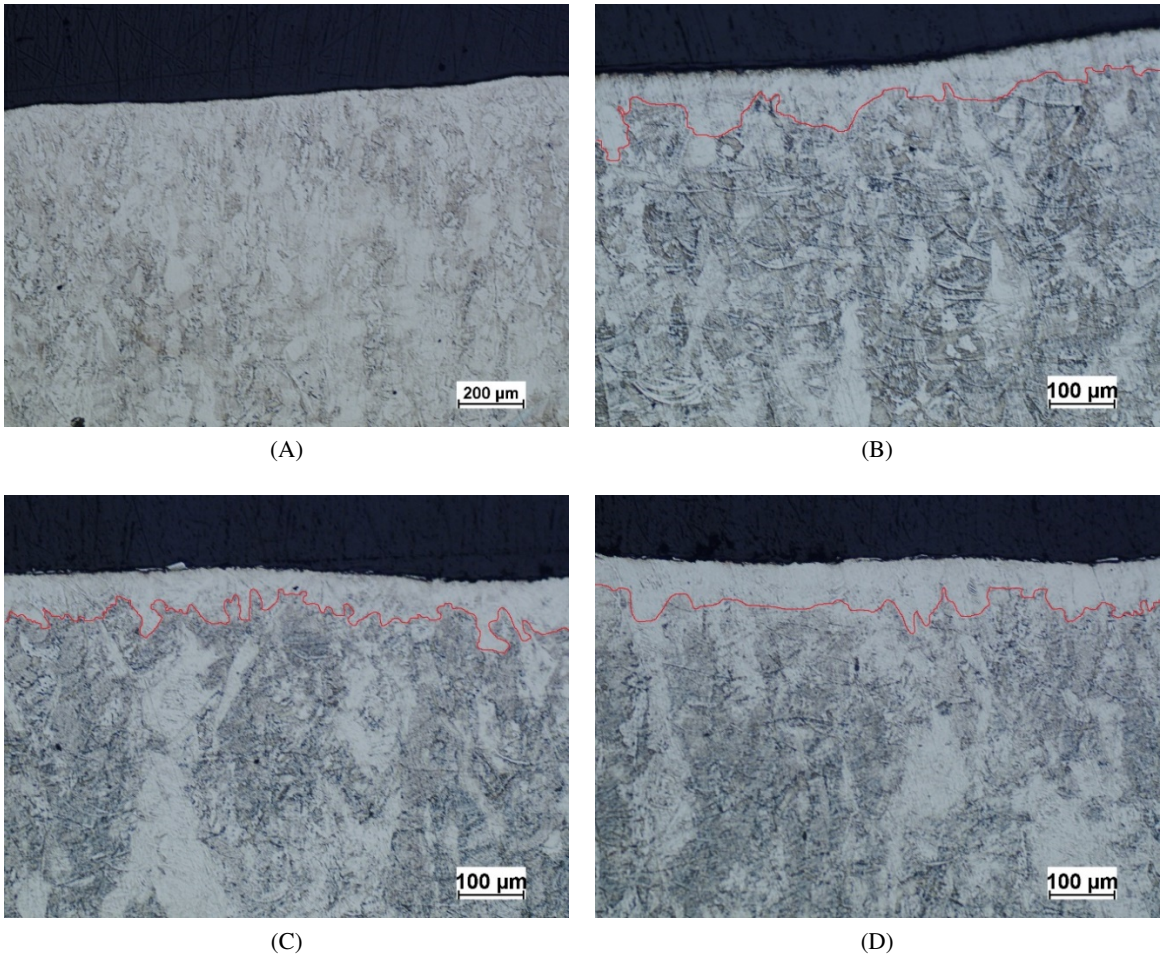

(A) (B)

(C) (D)

Fig. 6. The cross section of specimens showing modified surface layer after SP: (A) reference; (B) ceramic; (C) glass; (D) steel. SP, shot peening

ence sample. Qin et al. [9], on the other hand, detected that roughness increases with the application of higher peening pressure. For peening pressures of 0.24, 0.40, and 0.52 MPa, the R_a value was 2.47 $\pm$ 0.23, 3.38 $\pm$ 0.47, and 3.91 $\pm$ 0.36 µm, respectively. The roughness after the SP process also depends on the particle size, hardness, and condition of the treated surface. Roughness directly affects fatigue properties [43]. As the R_a parameter increases, the fatigue strength decreases at a constant stress level. Fatigue limit increases as the value of arithmetic mean roughness (R_a) decreases. Thus, the fatigue properties after the SP process should be improved.

3.4. Microstructure characterization

Figure 6 illustrates the subsurface layer before and after SP process.

Metallographic studies have shown differences in the surface layer after SP at a distance to which the microstructure has increased in hardness, distinguishing it from the base material. Etching with the Kalling reagent makes the martensite grains darker. Reagent #1 makes ferrite grains slightly darker while it does not attack austenite grains and carbides. Work hardened with fine deformed grains are visible in contrast to regular coarse grains beneath. In Figure 6, the red line indicates the layer distinguished from the base material below, but it is worth noting that the reinforced layer does

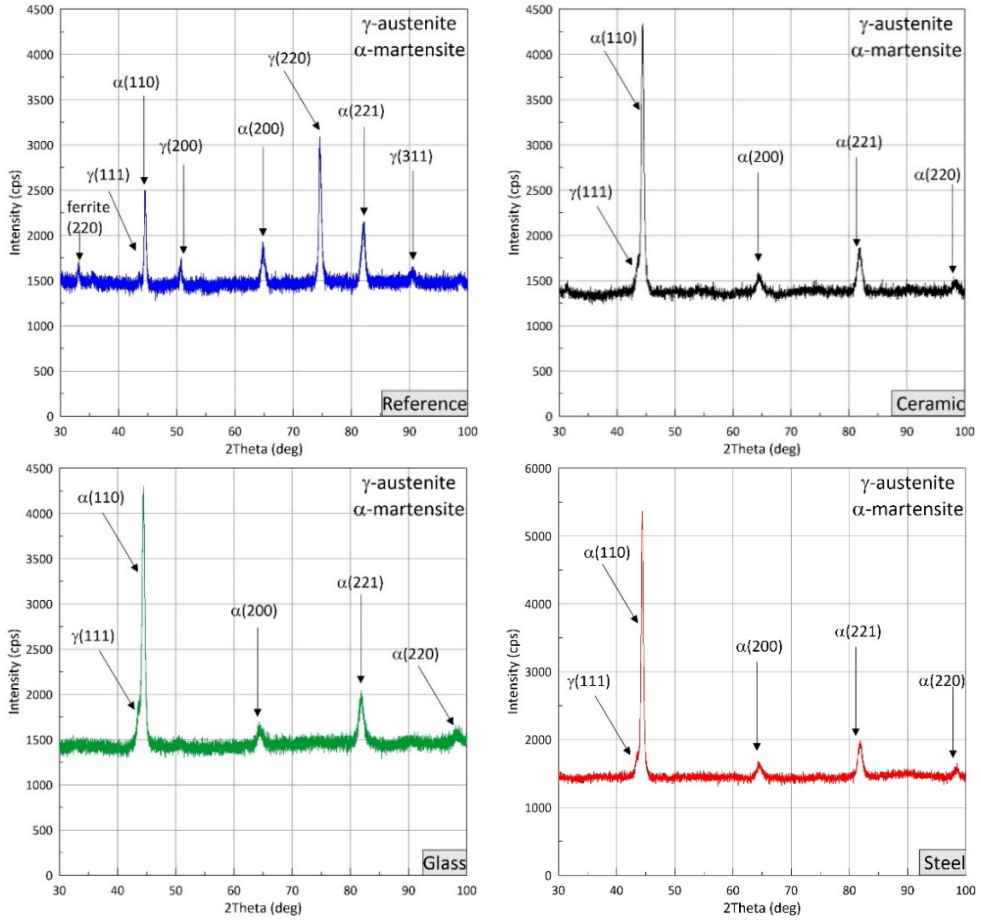

Fig. 7. Phase compositions of as-printed and shot peened samples, XRD. XRD, X-ray diffractometer

not correspond directly to the red line. Hardness should also be taken into consideration and reinforcement can be referred to both above and below the aforementioned line. Below that, perpendicular areas were revealed, representing the direction of cooling of the material. The microstructure shown in Figure 6 is perpendicular to the build direction and parallel to the print direction, while the SP is implemented parallel to the build direction. Cheruvathur et al. [44] detected a cellular-dendritic solidification microstructure in 17-4PH steel.

Three phases, γ-austenite, α-martensite, and δ-ferrite, were detected in the as-fabricated condition. In contrast, after peening, the spectrum changed, and two phases, γ-austenite and α-martensite, were detected (see Figure 7). The size of the crystallites was the highest for the reference sample, while after SP the largest crystallites were characterized by the steel-shot peened sample (see Table 3). The smallest crystallite size was detected for the sample shot peened with glass beads. The size of the crystallites does not directly correspond to the size of the grains; however, on that bases, assumptions can be made that there has been refinement of the grains as a common result of SP [45]. Only γ (111) peak was found after the SP process and some increase in the height of α martensite peak was observed, namely (110). There was also a visible reduction in austenite-derived peaks and growth of martensite peaks, suggesting a strain-induced transformation of residual austenite into martensite [46]. Slight shift in diffraction peaks for approximately 44° of 2θ may be attributed to change in phase composition or induction of compressive residual stresses in the material [47].

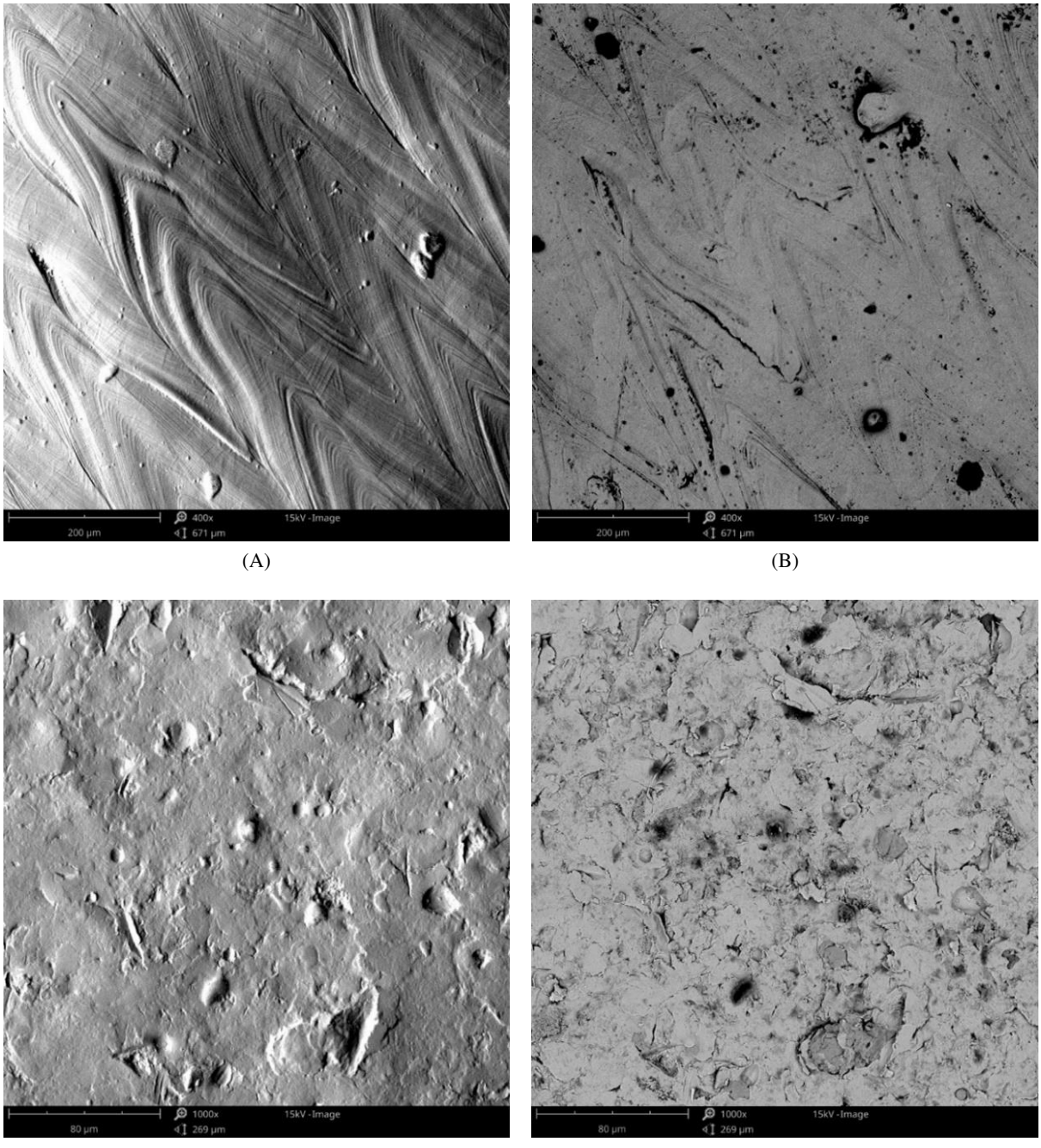

Fig. 8. Surface morphology of 17-4PH steel: (A) reference sample, SEM-topo mode; (B) reference, SEM-BSD mode; (C) ceramic, SEM-topo; (D) ceramic, BSD mode; (E) glass, SEM-topo; (F) glass, BSD mode; (G) steel SEM-topo; (H) steel, BSD mode. BSD, backscattered electrons; SEM, scanning electron microscopy

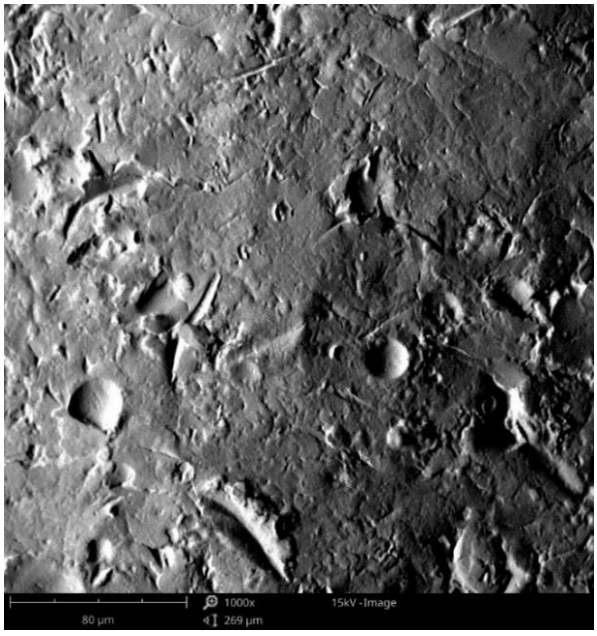

(E)

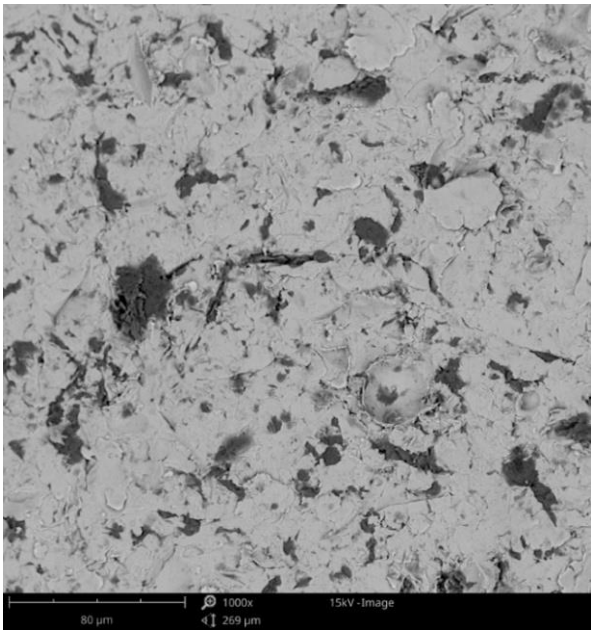

(F)

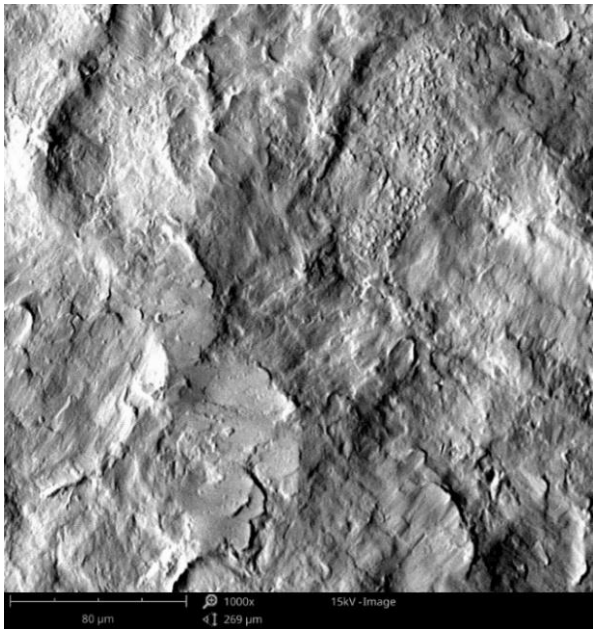

(G)

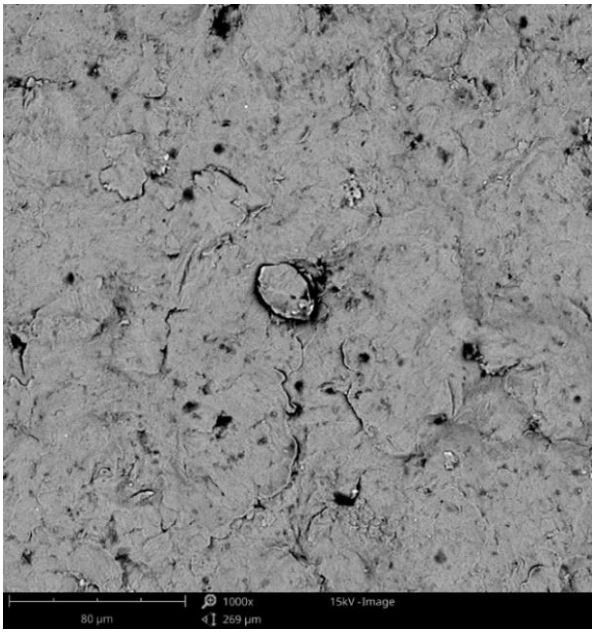

(H)

Fig. 8. ...continued

3.5. SEM-EDS analyses

Figure 8 shows micrographs of shot peened surfaces. SEM topographic and BSD modes have been employed to visualize the surface morphology development.

The topography of the material surface after SP differs significantly from that after AM. After AM, the melt pools, flow lines of the material, as well as the boundaries between laser beam passes are visible in Figure 8A. The surface resembles

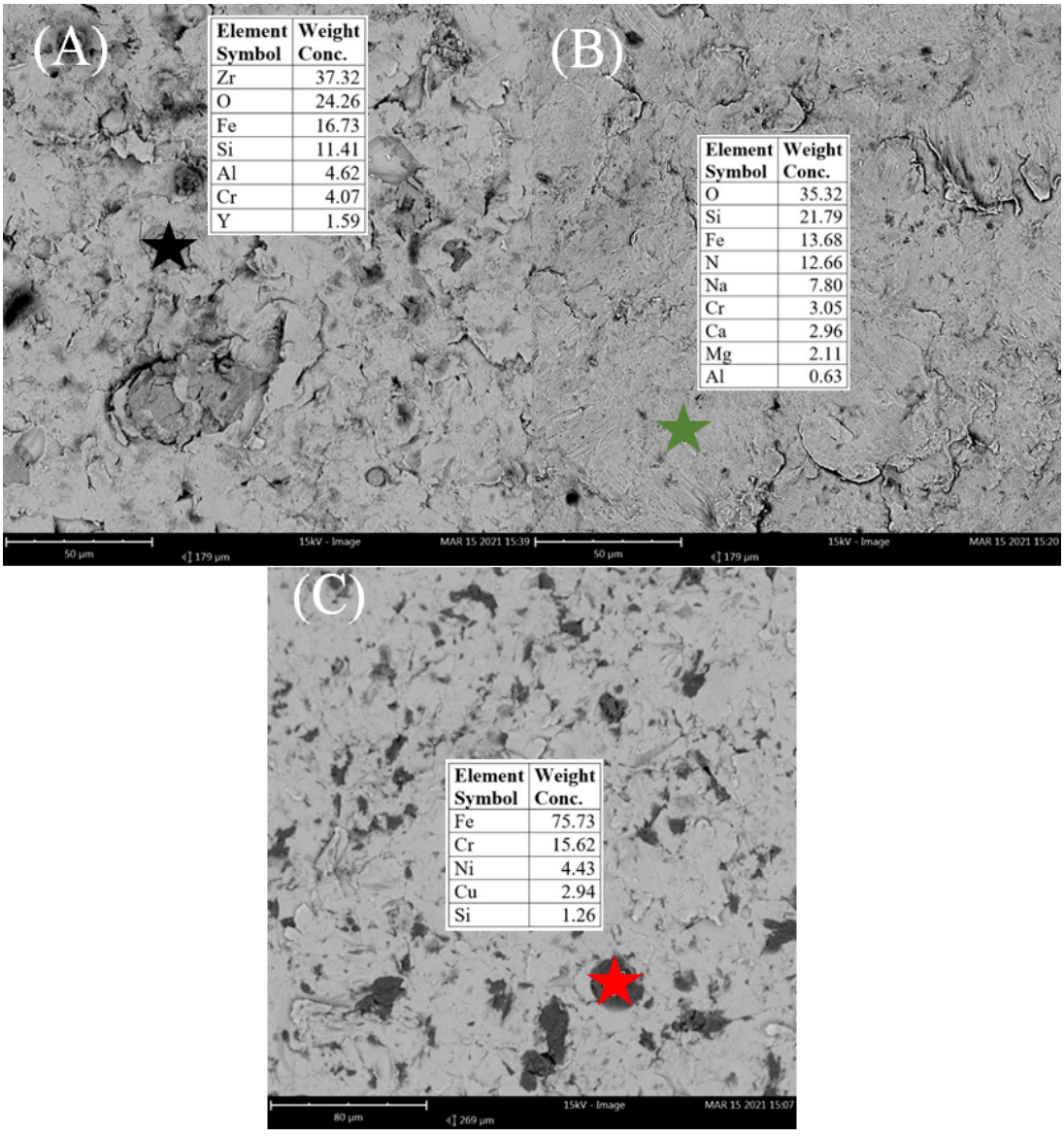

Fig. 9. Chemical composition spot analysis: (A) ceramic, (B) glass, (C) steel, SEM-EDS. EDS, energy dispersive X-ray spectroscopy; SEM, scanning electron microscopy

Table 3. Results of α-martensite crystallite size of unpenned and shoot penned 17-4PH steel using the ceramic, glass, and steel peening beads

Specimen	Position, [°2Th.]	Crystallite size [nm]
Ref.	44.53 (3)	25
Ceramic	44.36 (2)	16
Glass	44.40 (2)	15
Steel	44.37 (2)	19

"fish scales" with the laser beam paths overlapping by approximately 40%–50% at a half-width of approximately 100 μm. On the other hand, after the SP surface becomes more irregular, the surface of the material was plastically deformed by the particles hitting the surface, indentations produced by spherical shots, as well as those of irregular shape are visible. The shot particles can break the continuity of the material and thus cause it to splinter or cause small local cracks. The irregular shape of

Table 4. Electrochemical parameters of 17-4PH at different surface conditions in the 3.5 wt% NaCl solution

Sample	I_{corr} (μA/cm^2)	E_{corr} (V_{SCE})	E_{pit} (V_{SCE})
Ref.	0.799 ± 0.011	-0.214 ± 0.015	0.343 ± 0.018
Ceramic	0.660 ± 0.009	-0.207 ± 0.012	0.165 ± 0.015
Glass	0.227 ± 0.007	-0.180 ± 0.011	0.259 ± 0.021
Steel	0.019 ± 0.008	-0.054 ± 0.012	0.462 ± 0.014

SCE, saturated calomel electrode

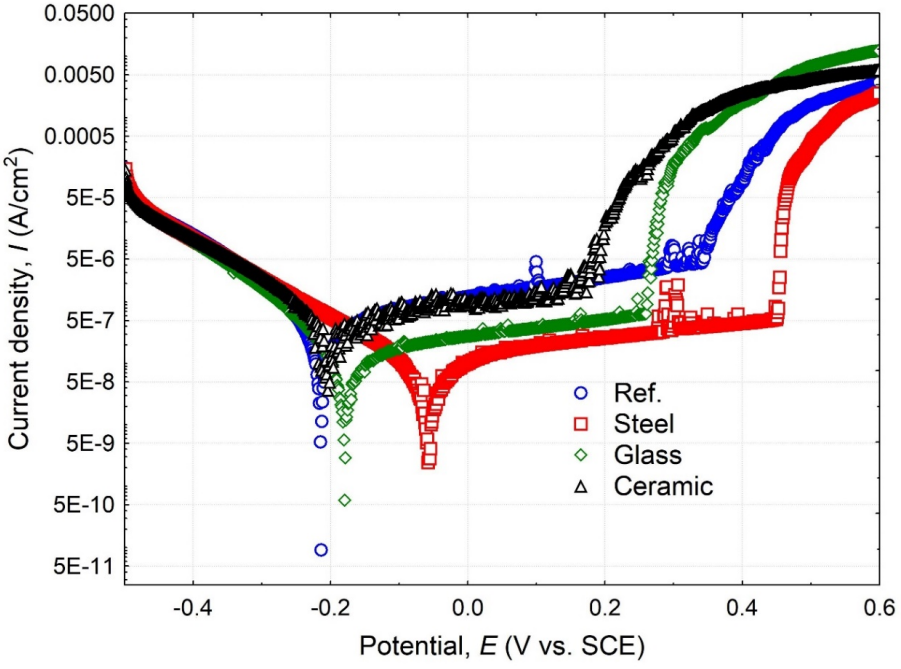

Fig. 10. Potentiodynamic polarization curves in 3.5% NaCl solution

some pits probably indicates the splitting of hard but brittle particles and, thus, their easier penetration into surfaces. The sheet particles or whole particles can sometimes get stuck in the surface and then be pressed in by subsequent impacting sheets. Similar conclusions were reached by Kameyama and Komotori [48]. It was found that powder particles can be locked and pressed into surfaces, and above that, particles could directly affect the local hardness by introducing local lamellar structures from shots particles. In the case of a glass peened surface, fragmentation of the peening medium is possible, the surface is slightly different from the rest of the surface after SP. It is also possible to locate glass fragments in the surface affecting the surface in contact with the corrosive environment.

EDS spot analysis (see Figure 9) confirmed the presence of ceramic and glass particles in the surface, but the presence of metallic particles could not be completely confirmed due to similar composition. In the sample treated by the ceramic shot, the presence of Zr, Si, O, and Al have been identified, which compares with the chemical composition of the ceramic beads given in Table 1. Similarly, in the case of glass peened surface, the presence of Si, Na, Mg, O, and Ca chemical elements agrees with the nominal chemical composition of the shot given in Table 1; such residual shots noted are typical and were found in previous research.

3.6. Corrosion testing

On the basis of the analysis of Tafel curves (Figure 10), an increase in the corrosion potential of E_{corr} after SP was observed, considering that the main parameter affecting resistance is I_{corr}. In terms of corrosion potential, the best performance of the surface shot peened with steel>glass>ceramics, respectively (see Table 4). When comparing with the previous research [42], a different solution was used: 3.5% wt. instead of 9%. The results of the tests also differ; previously, the best resistance was characterized by samples shot peened with ceramics, then with glass; in this case, the CrNi shots that gave a better result in terms of corrosion performance. As studies have shown, the effect of crystallite size on corrosion resistance can vary and depend on the size of the crystallites [49]. With a higher density of grain boundaries, more corrosion nucleation sites are formed [50]. However, a higher number of grain boundaries can positively affect the formation of a passive layer, and in the case of 17-4PH steel, the formation of a chromium-rich passive layer was demonstrated [28].

Lower roughness combined with crack closing mechanism affects more favorable electrochemical parameters. This behavior of the samples was mostly affected by the magnitude of the surface roughness (see Table 3), but also by crystallite size and the level of work hardening effect. When the plateau range is exceeded for all samples, there is a breakthrough potential E_{pit} after which pitting corrosion occurs.

4. Conclusions

Analysis of the chemical composition showed a composition in line with the requirements outlined in the standards ASTM A564, EN10088-1, as well as the manufacturer's declarations.

SP increased the hardness of the surface layer of 17-4PH steel produced by the DMLS technique, which combined with reduced roughness should translate into improved fatigue strength. After SP using glass beads, the highest hardness was obtained right beneath the surface at around 459 $HV_{0.2}$, with a slightly lower hardness obtained after using steel shots at 450 $HV_{0.2}$ and ceramics at 436 $HV_{0.2}$. The use of steel shots enabled to increase the hardness in the deepest part in the material. This is because the increase in hardness depends on the value of compressive residual stresses. The value of the compressive residual stress deep in the material depends on the energy of a single shot; a constant peening pressure therefore results from its mass.

The surface hardness was 241, 496, 522, and 501 $HV_{0.2}$ for Ref., ceramic, glass, and steel, respectively. It is worth noting here that structure defects such as pores, unmelted powder particles, inclusions or particles remaining after the SP process can directly affect the value of surface hardness.

A 7% and 12% reduction in *Ra* roughness after SP was achieved for ceramics and steel, respectively, demonstrating that SP can be an effective post-processing method after 3D printing. SP glass beads resulted in a 10% increase in roughness.

Three phases, γ-austenite, α-martensite, and ferrite, were detected in the as-fabricated condition. After peening two phases, γ-austenite and α-martensite, were detected in all of the samples. The size of the crystallites was smallest after processing with glass, 15 nm slightly larger sizes were obtained after using ceramics at 16 nm. The largest size of crystallites was obtained for Ref. After peening, the largest size of crystallites was characterized by the sample processed using steel shots.

The steel texture was typical for additively manufactured steel. Longitudinal notches caused by fragmentation of the medium are visible, as well as indentations from spherical particles, especially in the case of the glass peened sample. The surface topography changed after peening, and the strengthening in the near-surface layer reached 40, 60, and 80 μm for ceramic, glass, and steel, respectively.

EDS analysis confirmed the presence of residual particles used for SP in the structure, which can change material properties after SP.

The highest performance in terms of corrosion resistance after SP was obtained consecutively for steel, glass, and ceramics. Roughness had the greatest effect on corrosion resistance; lower roughness influences more favorable electrochemical parameters. The effect of crystallite size was also noted

for larger crystallites in the structure after SP had a favorable impact on corrosion performance. The tests confirmed the good mechanical properties of 17-4PH steel combined with relatively high corrosion resistance.

References

[1] Wang J, Zou H, Li C, Peng Y, Qiu S, Shen B. The microstructure evolution of type 17-4PH stainless steel during long-term aging at 350°C. *Nucl Eng Des*. 2006;236(24): 2531–6.

[2] Sabooni S, Chabok A, Feng SC, Blaauw H, Pijper TC, Yang HJ, et al. Laser powder bed fusion of 17–4 PH stainless steel: a comparative study on the effect of heat treatment on the microstructure evolution and mechanical properties. *Addit Manuf*. 2021;46: 102176.

[3] Slunder CJ, Hoenie AF, Hall AM. Thermal and mechanical treatment for precipitation-hardening stainless steels. Battelle Memorial Inst Columbus Ohio Columbus labs; 1968 Jan.

[4] Hsiao CN, Chiou CS, Yang JR. Aging reactions in a 17-4 PH stainless steel. *Mater Chem Phys*. 2002;74(2): 134–42.

[5] Sowa R, Kowal A, Roga E, Arabasz S, Dziedzic A, Dul I, et al. Influence of double solution treatment on hardness in 17-4 pH steel. *Zas Mat*. 2015;56(3): 261–8.

[6] Sealy MP, Karunakaran R, Ortgies S, Madireddy G, Malshe AP, Rajurkar KP. Reducing corrosion of additive manufactured magnesium alloys by interlayer ultrasonic peening. *CIRP Ann*. 2021;70(1): 179–82.

[7] Wang C, Wang C, Wang L, Lai Y, Li K, Zhou Y. A dislocation density–based comparative study of grain refinement, residual stresses, and surface roughness induced by shot peening and surface mechanical attrition treatment. *Int J Adv Manuf Technol*. 2020;108(1–2): 505–25.

[8] Świetlicki A, Szala M, Walczak M. Effects of shot peening and cavitation peening on properties of surface layer of metallic materials—A short review. *Materials*. 2022;15(7): 2476.

[9] Qin E, Chen G, Tan Z, Wu S. Shot peening and thermal stress relaxation in 17-4 PH stainless steel. *J Mater Eng Perform*. 2015;24(11): 4578–83.

[10] Nino-Barrera J, Sanchez-Aleman J, Acosta-Humanez M, Gamboa-Martinez L, Cortes-Rodriguez C. Shot peening increases resistance to cyclic fatigue fracture of endodontic files. *Sci Rep*. 2021;11(1): 12961.

[11] Żebrowski R, Walczak M, Korga A, Iwan M, Szala M. Effect of shot peening on the mechanical properties and cytotoxicity behaviour of titanium implants produced by 3D printing technology. *J Healthcare Eng*. 2019;2019: 1–11.

[12] John M, Kalvala PR, Misra M, Menezes PL. Peening techniques for surface modification: processes, properties, and applications. *Materials*. 2021;14(14): 3841.

[13] Sadeghi E, Pant P, Jafari R, Peng RL, Karimi P. Subsurface grain refinement in electron beam-powder bed fusion of Alloy 718: surface texture and oxidation performance. *Mater Charact*. 2020;168: 110567.

[14] Leon A, Katarivas Levy G, Ron T, Shirizly A, Aghion E. The effect of strain rate on stress corrosion performance of Ti6Al4V alloy produced by additive manufacturing process. *J Mater Res Technol*. 2020;9(3): 4097–105.

[15] Wen D, Long P, Li J, Huang L, Zheng Z. Effects of linear heat input on microstructure and corrosion behavior of an austenitic stainless steel processed by wire arc additive manufacturing. *Vacuum*. 2020;173: 109131.

[16] Hung W. Postprocessing of additively manufactured metal parts. *J Mater Eng Perform*. 2021;30(9): 6439–60.

[17] Maleki E, Bagherifard S, Bandini M, Guagliano M. Surface post-treatments for metal additive manufacturing: progress, challenges, and opportunities. *Addit Manuf*. 2021;37: 101619.

[18] AlMangour B, Yang JM. Improving the surface quality and mechanical properties by shot-peening of 17-4 stainless steel fabricated by additive manufacturing. *Mater Des*. 2016;110: 914–24.

[19] Tavares SSM, Pardal JM, Martins TRB, da Silva MR. Influence of sulfur content on the corrosion resistance of 17-4PH stainless steel. *J Mater Eng Perform*. 2017;26(6): 2512–9.

[20] Fargas G, Roa JJ, Mateo A. Effect of shot peening on metastable austenitic stainless steels. *Mater Sci Eng A*. 2015;641: 290–6.

[21] Kirk D, Payne NJ. Transformations induced in austenitic stainless steels by shot peening. In: *ICSP7: 7th International Conference on Shot Peening*, Warsaw, Poland; 1999.

[22] Murr LE, Martinez E, Hernandez J, Collins S, Amato KN, Gaytan SM, et al. Microstructures and properties of 17-4 PH stainless steel fabricated by selective laser melting. *J Mater Res Technol*. 2012;1(3): 167–77.

[23] Starr TL, Rafi K, Stucker B, Scherzer CM. Controlling phase composition in selective laser melted stainless steels. 2012 Aug 22 [cited 2022 Nov 29] Available from: `https://repositories.lib.utexas.edu/handle/2152/88426`

[24] Rafi HK, Pal D, Patil N, Starr TL, Stucker BE. Microstructure and mechanical behavior of 17-4 precipitation hardenable steel processed by selective laser melting. *J Mater Eng Perform*. 2014;23(12): 4421–8.

[25] Guo D, Chen J, Chen X, Shi Q, Cristino VAM, Kwok CT, et al. Pitting corrosion behavior of friction-surfaced 17-4PH stainless steel coatings with and without subsequent heat treatment. *Corros Sci*. 2021;193: 109887.

[26] Stoudt MR, Campbell CE, Ricker RE. Examining the relationship between post-build microstructure and the corrosion resistance of additively manufactured 17-4PH stainless steel. *Materialia*. 2022;22: 101435.

[27] Campbell CE, Stoudt MR, Zhang F. Additive manufacturing of steels and stainless steels. In: Bourell DL, Frazier W, Kuhn H, Seifi M. (eds.) *Additive manufacturing processes*: ASM International; 2020. p. 346–65 [cited 2022 Aug 31]. Available from:

http://dl.asminternational.org/handbooks/book/119/chapter/2349634/Additive-Manufacturing-of-Steels-and-Stainless

[28] Lara Banda M del R, Pérez Ortíz DY, Gaona Tiburcio C, Zambrano-Robledo P, Cabral Miramontes JA, Almer aya Calderon F. Citric acid passivation of 15-5PH and 17-4PH stainless steel used in the aeronautical industry. In: Zambrano-Robledo P, Salinas-Rodriguez A, Almeraya Calderon F. (eds). *Proceedings of the Symposium of Aeronautical and Aerospace Processes, Materials and Industrial Applications*. Cham: Springer International Publishing; 2018. p. 95–104 [cited 2022 Jun 8]. Available from: http://link.springer.com/10.1007/978-3-319-65611-3_9

[29] Karaminezhaad M, Sharafi S, Dalili K. Effect of molybdenum on SCC of 17-4PH stainless steel under different aging conditions in chloride solutions. *J Mater Sci*. 2006;41(11): 3329–33.

[30] Coseglio MSDR. Sulphide stress cracking of 17-4 PH for applications in oilfield components. *Mater Sci Technol*. 2017;33(16): 1863–78.

[31] Nakhaie D, Moayed MH. Pitting corrosion of cold rolled solution treated 17-4 PH stainless steel. *Corros Sci*. 2014;80: 290–8.

[32] Raja KS, Rao KP. Pitting behavior of type 17-4 PH stainless steel weldments. *Corrosion*. 1995;51(8): 586–92.

[33] Kosasang O, Wongkaewmoon M, Chumphongphan S. Effect of aging heat treatment on corrosion behavior and corrosion kinetics of 17-4PH stainless steel in artificial saliva. *J Sains Malays*. 2021;50(3): 849–58.

[34] Barroux A, Ducommun N, Nivet E, Laffont L, Blanc C. Pitting corrosion of 17-4PH stainless steel manufactured by laser beam melting. *Corro Sci*. 2020;169: 108594.

[35] Lashgari HR, Xue Y, Onggowarsito C, Kong C, Li S. Microstructure, tribological properties and corrosion behaviour of additively manufactured 17-4PH stainless steel: effects of scanning pattern, build orientation, and single vs. double scan. *Mater Today Commun*. 2020;25: 101535.

[36] Jacob G. *Prediction of solidification phases in Cr-Ni stainless steel alloys manufactured by laser based powder bed fusion process*. Gaithersburg, MD: National Institute of Standards and Technology; 2018 Mar p. NIST AMS 100-14. Report Number: NIST AMS 100-14.

[37] Eskandari H, Lashgari HR, Ye L, Eizadjou M, Wang H. Microstructural characterization and mechanical properties of additively manufactured 17–4PH stainless steel. *Mater Today Commun*. 2022;30: 103075.

[38] Wang Z, Luan W, Huang J, Jiang C. XRD investigation of microstructure strengthening mechanism of shot peening on laser hardened 17-4PH. *Mater Sci Eng A*. 2011;528(21): 6417–25.

[39] Mathoho I, Akinlabi ET, Arthur N, Tlotleng M, Masina B. Metallurgical characteristics of laser peened 17-4 PH SS processed by LENS technique. In: The Minerals, Metals & Materials Series (eds) *TMS 2019 148th Annual Meeting & Exhibition Supplemental Proceedings*. Cham: Springer International Publishing; 2019. p. 279–85. (The Minerals, Metals & Materials Series).

[40] Bagherifard S, Ghelichi R, Guagliano M. Numerical and experimental analysis of surface roughness generated by shot peening. *Appl Surf Sci*. 2012;258(18): 6831–40.

[41] Higounenc O. Correlation of shot peening parameters to surface characteristic. 2005. In: *ICSP9: 9th International Conference on Shot Peening*, Marne la Vallée, France, 6-9.09.2005.

[42] Walczak M, Szala M. Effect of shot peening on the surface properties, corrosion and wear performance of 17-4PH steel produced by DMLS additive manufacturing. *Archiv Civ Mech Eng*. 2021;21(4): 157.

[43] Sanaei N, Fatemi A. Analysis of the effect of surface roughness on fatigue performance of powder bed fusion additive manufactured metals. *Theor Appl Fract Mech*. 2020;108: 102638.

[44] Cheruvathur S, Lass EA, Campbell CE. Additive manufacturing of 17-4 PH stainless steel: post-processing heat treatment to achieve uniform reproducible microstructure. *JOM*. 2016;68(3): 930–42.

[45] Maleki E, Unal O, Reza Kashyzadeh K, Bagherifard S, Guagliano M. A systematic study on the effects of shot peening on a mild carbon steel: microstructure, mechanical properties, and axial fatigue strength of smooth and notched specimens. *Appl Surf Sci Adv*. 2021;4: 100071.

[46] Guennouni N, Barroux A, Grosjean C, Maisonnette D, Nivet E, Andrieu E, et al. Comparative study of the microstructure between a laser beam melted 17-4PH stainless steel and its conventional counterpart. *Mater Sci Eng A*. 2021;823: 141718.

[47] Efe Y, Karademir I, Husem F, Maleki E, Karimbaev R, Amanov A, et al. Enhancement in microstructural and mechanical performance of AA7075 aluminum alloy via severe shot peening and ultrasonic nanocrystal surface modification. *Appl Surf Sci*. 2020;528: 146922.

[48] Kameyama Y, Komotori J. Effect of micro ploughing during fine particle peening process on the microstructure of metallic materials. *J Mater Process Technol*. 2009;209(20): 6146–55.

[49] Soleimani M, Mirzadeh H, Dehghanian C. Effect of grain size on the corrosion resistance of low carbon steel. *Mater Res Express*. 2020;7(1): 016522.

[50] Qiao M, Hu J, Guo K, Wang Q. Influence of shot peening on corrosion behavior of low alloy steel. *Mater Res Express*. 2020;7(1): 016574.

Received 2022-10-10
Accepted 2023-01-05